Tensor network formulation of the massless Schwinger model with staggered fermions

Nouman Butt,[1,*] Simon Catterall,[1] Yannick Meurice,[2] Ryo Sakai,[2] and Judah Unmuth-Yockey[1,†]

[1]*Department of Physics, Syracuse University, Syracuse, New York 13244, USA*
[2]*Department of Physics and Astronomy, The University of Iowa, Iowa City, Iowa 52242, USA*

(Received 14 January 2020; accepted 7 May 2020; published 26 May 2020)

We construct a tensor network representation of the partition function for the massless Schwinger model on a two-dimensional lattice using staggered fermions. The tensor network representation allows us to include a topological term. Using a particular implementation of the tensor renormalization group we calculate the average plaquette and topological charge density for the theory. For a range of values of the coupling constant for the topological term, Θ, and the gauge coupling, β, we compare with results from hybrid Monte Carlo simulations when possible and find good agreement. In order to further understand the role of fermions and topology in this model, we compare calculations of the same observables in a similar model, the Abelian Higgs model.

DOI: 10.1103/PhysRevD.101.094509

I. INTRODUCTION

In recent years there has been a surge of interest in applying tensor network methods to calculate the properties of lattice spin and gauge models [1–10]. In low dimensions these formulations can avoid the usual sign problems associated with negative or complex probability weights that plague Monte Carlo (MC) approaches and can yield very efficient computational algorithms [11–16]. For compact fields the general strategy has been to employ character expansions for all Boltzmann factors occurring in the partition function and subsequently to integrate out the original fields, yielding an equivalent formulation in terms of integer—or half-integer—valued fields which can be interpreted as the indices of local tensors. The indices of these local tensors are then contracted (summed over), from which one recovers the full partition function.

However, writing local tensors for models with relativistic lattice fermions is more complicated [17–22]. One reason is tied to the Grassmann nature of the fermions which can induce additional, nonlocal sign problems which may be hard to generate from local tensor contractions. However, Gattringer *et al.* have shown in Ref. [23] that a suitable dual formulation can be derived in the case of the massless Schwinger model which is free of these sign problems. Using this dual representation they have formulated a general Monte Carlo algorithm that can be used to simulate the model even in the presence of nonzero chemical potential and topological terms [24].

Other directions into the investigation of the Schwinger model have appeared in recent years as well. One approach has been the use of other numerical renormalization group methods like the density matrix renormalization group (DMRG) with matrix product states or matrix product operators (MPS or MPO). The massive Schwinger model with staggered fermions was investigated in Ref. [25] using the DMRG. In Ref. [26] the mass spectrum of the Schwinger model was calculated at zero and finite mass, and in Ref. [27] the authors studied the Schwinger model at finite temperature using the DMRG with MPO. The effect of truncation on the number of representations retained in the electric field basis for the Schwinger model was investigated in Ref. [28]. In Ref. [29] the confinement properties of the Schwinger model in the presence of a topological term were studied, and in Ref. [30] the authors considered the effects of a topological term on the vacuum structure of the model, again using the DMRG.

Similarly, Ref. [31] looked at a $\mathbb{Z}_n$ formulation of the Schwinger model using the DMRG. They found that at large n, one recovers similar results to the original continuous $U(1)$ symmetry in the Schwinger model. Out of equilibrium properties were looked at in Ref. [32] for that same model.

In addition, proposals and investigations into the potential for quantum simulations and computations of the Schwinger model were done in Refs. [33–39], and an actual experimental implementation carried out in Ref. [40]. Besides trapped-ion approaches, experiments

*ntbutt@syr.edu
†jfunmuthyockey@gmail.com

with Rydberg atoms are being explored as a potential tool for quantum computation [41]. References [33,34] carried out initial feasibility and practicality studies surrounding the quantum computation of the Schwinger model using trapped-ions, or superconducting qubits. In Ref. [36] the lattice Schwinger model was considered for quantum simulation using cold atoms in an optical lattice. In Ref. [37] the authors considered general $U(1)$ lattice gauge theories, and they integrate out the gauge degrees of freedom, being left with a model of strictly matter, interacting nonlocally [42]. In Ref. [35], the authors considered the joint computation of the lattice Schwinger model using classical and quantum computers.

More recently, classical computations simulating quantum computations of the Schwinger model have been carried out. In Refs. [38,39] the vacuum Θ-angle was studied in small systems using computing libraries which mimic the behavior of current, and near-term, quantum computers, quantifying the quantum-computational cost for a future study of the Schwinger model with a (time-varying) Θ term.

In this paper we show that the dual world-line formulation from Ref. [23] can be replicated by contraction of a suitable tensor network. It should be noted that a tensor formulation of the model allows for the definition of a transfer matrix, quantum Hamiltonian, and local Hilbert space. Rather than following a Monte Carlo strategy we instead use and follow the philosophy of the tensor renormalization group to coarse grain this tensor network. Important steps in tackling relativistic fermions with tensor networks were taken in Refs. [18–20]. There the Schwinger model with Wilson fermions was approached by using the Grassmann tensor renormalization group method, where the Grassmann variables are coarse-grained, as well as the local tensors [43]. From the tensor network formulation we calculate the partition function and free energy. We show that the results agree well with both Ref. [24] and conventional hybrid Monte Carlo simulations where the latter can be performed.

We start by reviewing the construction of the dual representation in Sec. II and show how the resulting dimer/loop representation can be obtained by the contraction of a suitable tensor network. In Sec. III we present the form of a transfer matrix for this model in terms of the local tensors in the tensor network. Then we derive the form of the fundamental tensor that is needed for the higher-order tensor renormalization group (HOTRG) algorithm [16] in Sec. IV. In Sec. V we describe the results of a coarsening of this tensor network using the HOTRG algorithm, calculate the free energy and its derivatives and compare the results to Monte Carlo simulations. Subsequently we go on to add a topological term to the action with coupling Θ. Finally, to compare with Schwinger model results, we compute the same expectation values for a different model, the Abelian Higgs model, in Sec. VI. We conclude in Sec. VII with a summary of the advantages and disadvantages of the method in this context.

II. MASSLESS SCHWINGER MODEL AND ITS DUAL REPRESENTATION

We begin with the one-flavor staggered action for the massless Schwinger model on a two-dimensional space-time (Euclidean) lattice with N_s spatial sites, N_τ temporal sites, and a total volume $V \equiv N_s \times N_\tau$. The action is given by

$$S = S_F + S_g \tag{1}$$

with

$$S_F = \frac{1}{2}\sum_x \sum_{\mu=1}^{2} \eta_\mu(x)[\bar{\psi}(x)U_\mu(x)\psi(x+\mu) - \bar{\psi}(x+\mu)U_\mu^\dagger(x)\psi(x)] \tag{2}$$

and

$$S_g = -\beta \sum_x \mathrm{Re}[U_P(x)]. \tag{3}$$

The Abelian gauge field, $U_\mu(x) = e^{iA_\mu(x)}$, lives on the link between lattice sites x and $x+\mu$ and the fermions $\psi(x)$ and $\bar{\psi}(x)$ live at the sites. Here $\eta_\mu(x)$ is the staggered phase which for $\eta_1(x) = 1$ and $\eta_2(x) = (-1)^{x_1}$ with x_1 the $\hat{1}$-component of x. U_P is the usual Wilson plaquette operator $U_P(x) = \sum_{\mu<\nu} U_\mu(x)U_\nu(x+\mu)U_\mu^\dagger(x+\nu)U_\nu^\dagger(x)$. The partition function for this model is then given by

$$Z = \int D[U]D[\bar{\psi}]D[\psi]e^{-S} = \int D[U]e^{\beta\sum_x \mathrm{Re}[U_P(x)]}Z_F(U) \tag{4}$$

with $\int D[U] = \prod_x \int_{-\pi}^{\pi} dA_\mu(x)/2\pi$, $\int D[\bar{\psi}]D[\psi] = \prod_x \int d\bar{\psi}\times(x)d\psi(x)$, and Z_F represents the part of the partition function that depends on the fermion fields.

Following Ref. [23], and using the same notation for clarity, we first integrate out the fermions and generate an effective action depending only on the gauge fields. As a first step we redefine the link variables such that the staggered fermion phases $\eta_\mu(x)$ can be absorbed into modified link variables $U_\mu(x) \to \eta_\mu(x)U_\mu(x)$. Under this transformation the gauge action picks up an overall negative sign but the measure is invariant. The Boltzmann factor associated with each bilinear fermion term can be written as the product of forward and backward hopping terms yielding a partition function,

$$Z_F = \int D[U]D[\bar{\psi}]D[\psi] \times \prod_x \sum_{k=0}^{1} \left(-\frac{1}{2}\bar{\psi}(x)U_\mu(x)\psi(x+\mu)\right)^k \times \sum_{\bar{k}=0}^{1} \left(\frac{1}{2}\bar{\psi}(x+\mu)U_\mu^\dagger(x)\psi(x)\right)^{\bar{k}}. \quad (5)$$

Notice that higher order terms in the expansion of the Boltzmann factors vanish because of the Grassmann nature of the fermions. There are several ways to generate a nonzero contribution to Z_F. In each case, the Grassmann integration at each site must be saturated. To saturate the Grassmann integrations, exactly one forward and one backward hopping term must be associated with each site. This gives rise to a simple collection of possibilities. On the one hand, there may be a single forward and backward hop along the same link. This obviously saturates the integration and is referred to as a dimer. On the other hand, there may be a forward and backward hop on two different links at a site. This indicates the passage of fermionic current through the site, and again saturates the integration measure there. Furthermore because of gauge invariance any nondimer contribution to Z_F must correspond to a closed loop. Figure 1 shows the allowed site contributions. A bold link indicates the presence of a $\frac{1}{2}U$ or a $-\frac{1}{2}U^\dagger$ factor along that link. Notice that the links are oriented corresponding to the presence of an arrow on each bold link whose direction is conserved through a site.

For a loop ℓ with length $L(\ell)$ one finds a contribution with absolute value,

$$\left(\frac{1}{2}\right)^{L(\ell)} \prod_{x,\mu\in\ell} (U_\mu)^{k_\mu(x)} (U_\mu^\dagger)^{\bar{k}_\mu(x)}, \quad (6)$$

where only a single $k_\mu(x)$ or $\bar{k}_\mu(x)$ is nonzero per link. In addition each loop carries a certain Z_2 phase which depends on the length of the loop and its winding, $W(\ell)$, along the temporal direction given by

$$-(-1)^{\frac{1}{2}L(\ell)}(-1)^{W(\ell)}. \quad (7)$$

Here, the overall negative sign is the usual one for closed fermion loops while the second factor keeps track of the number of forward hops which is exactly half the total length of the loop for a closed loop. Finally the factor $(-1)^{W(\ell)}$ of the loop will be determined by the number of windings of the loop along the temporal direction assuming antiperiodic boundary conditions for the fermions. Using dimers (d) and loops (ℓ) as basic constituents for nonzero contributions to the fermionic partition function we can write

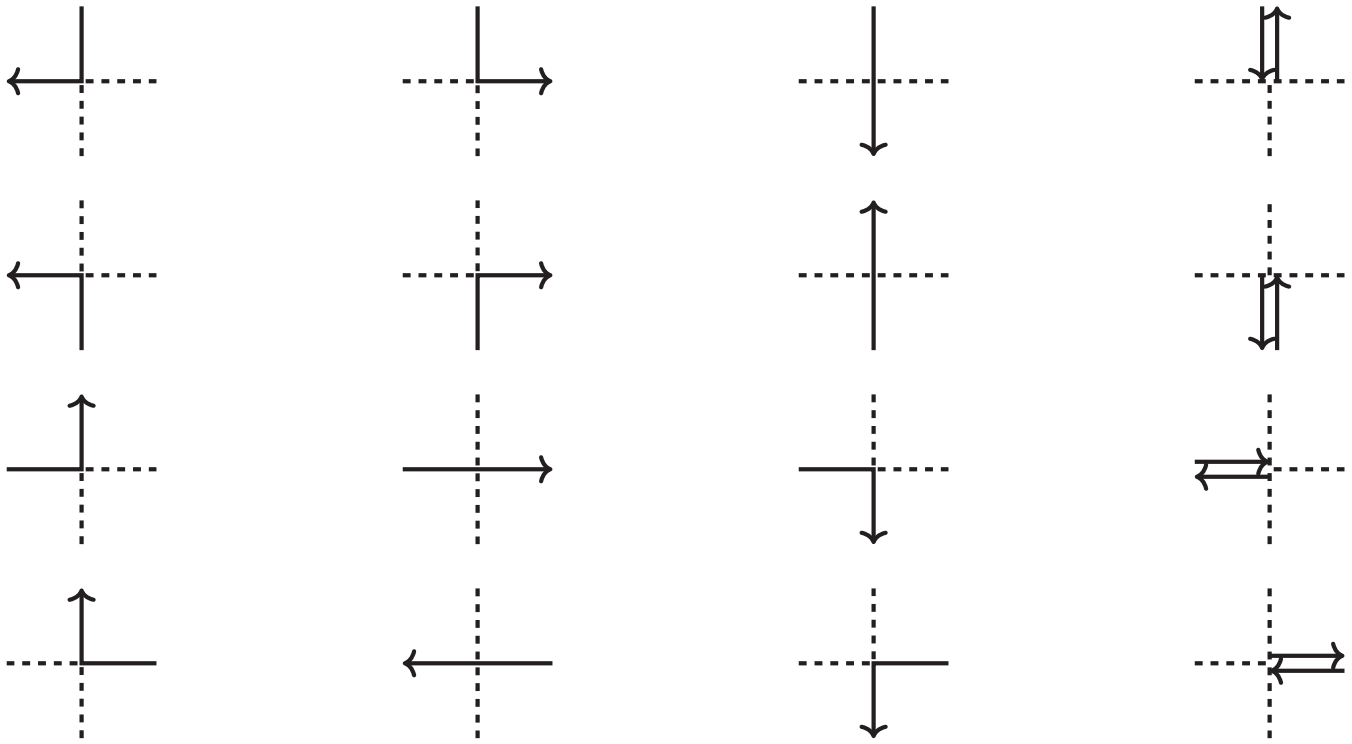

FIG. 1. Sixteen nonzero possibilities for $\psi, \bar{\psi}$ integration at a site. These 16 possibilities end up being exactly the nonzero elements of the fermion tensor.

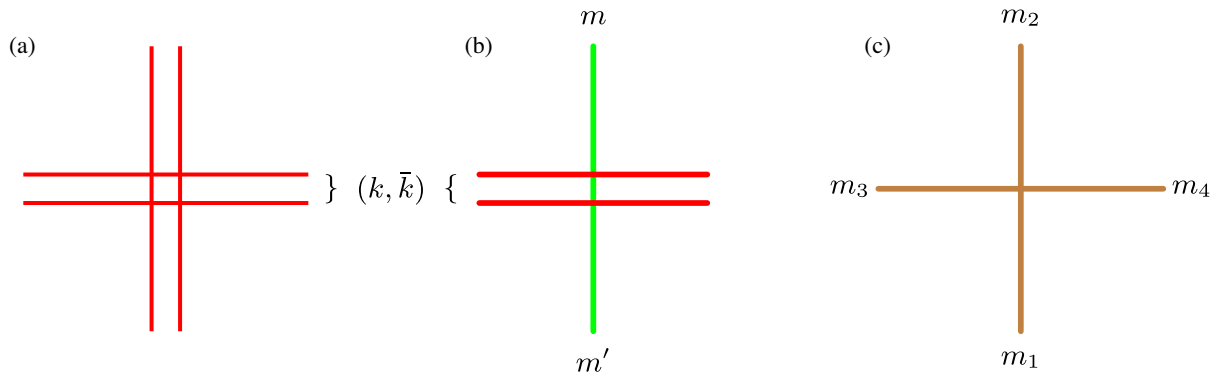

FIG. 2. (a) Fermion tensor associated with the sites of the lattice. The two lines in each direction can take on the values of unoccupied, or occupied with a forward or backwards current. Each pair can then have four states, unoccupied, outgoing fermionic current, incoming fermionic current, and both outgoing and incoming current, i.e., a dimer. (b) The constraint tensor associated with the links. This tensor enforces that the difference between the m electric field numbers appropriately matches, and compensates, the fermionic current across the link. (c) The gauge field tensor associated with each plaquette. This tensor has four indices, but the only nonvanishing elements are when all indices take the same value; i.e., it is diagonal in all four indices. Each nonzero element is associated with weight factors given by modified Bessel functions.

$$Z_F = \left(\frac{1}{2}\right)^V \sum_{\{\ell,d\}} (-1)^{N_L + \frac{1}{2}\sum_\ell L(\ell) + \sum_\ell W(\ell)} \times \prod_\ell \left[\prod_{x,\mu \in \ell} (U_\mu)^{k_\mu(x)}(x)(U_\mu^\dagger)^{\bar{k}_\mu(x)}(x) \right], \tag{8}$$

where N_L is the number of loops, and $\sum_{\{\ell,d\}}$ is a sum over all valid loop and dimer configurations. To proceed further we will need to construct this loop representation from the contraction of more basic objects located at sites, and we take up this task in the next section.

A. Tensor formulation of the fermionic partition function

We need to construct a local tensor which under contraction along lattice links yields Z_F. Let us ignore the overall sign for now and just deal with the magnitude. We allow two types of indices per link to capture separately the incoming and outgoing fermion lines making the fermion site tensor a rank eight object. To write down a tensor, first, let us fix the coordinates so that right and up are positive (no bar), and left and down are negative (bar). Since each site is either the end point of a dimer, or has fermionic current incoming and outgoing from it, then we can model this with the tensor structure (we leave off the gauge link factors for now),

$$T^x_{k_1\bar{k}_1 k_2 \bar{k}_2 k_3 \bar{k}_3 k_4 \bar{k}_4} = \begin{cases} 1 & \text{if } k_1 + k_4 + \bar{k}_2 + \bar{k}_3 = 1 \text{ and } k_2 + k_3 + \bar{k}_1 + \bar{k}_4 = 1 \\ 0 & \text{otherwise} \end{cases}, \tag{9}$$

where each $(k_i, \bar{k}_i) = 0, 1$. In order to reduce index clutter, we have made the replacement $k_1{:}k_1(x - \hat{1})$, $k_2{:}k_1(x)$, $k_3{:}k_2(x)$, $k_4{:}k_2(x - \hat{2})$, and similarly with the barred ks. This corresponds to an index ordering (left, right, up, down). A graphical representation of this tensor is shown in Fig. 2(a). By repeatedly contracting this site tensor with copies of itself over the lattice it can be seen that we generate the full set of closed loops and dimers for the model at zero gauge coupling excluding the overall factor of minus one for each closed fermion loop. The absolute value of the partition function at zero gauge coupling is then,

$$Z_F^{\beta=\infty} = \sum_{\{k,\bar{k}\}} \prod_x T^x_{k_1\bar{k}_1 k_2 \bar{k}_2 k_3 \bar{k}_3 k_4 \bar{k}_4}. \tag{10}$$

Here, $\{k, \bar{k}\}$ denote the set of $k, \bar{k}$ values for the entire lattice. Said another way, the 16 possible vertex configurations for fermion hopping in Fig. 1 are captured as nonzero tensor elements in the T tensor.

B. Integrating out the gauge fields

The fermion partition function in the previous section does not include any contribution or interaction with the gauge fields. To proceed further we will employ a character expansion of the Boltzmann factors associated with the gauge action. This will ensure that each plaquette in the lattice will carry an integer variable. Integration of the link gauge field in the background of a particular set of fermion

loops restricts the plaquette variables to change by plus or minus one on crossing any fermion line.

In this section, we will describe this in detail and, along with the tensor from the previous section, construct a tensor network that when fully contracted reproduces the full partition function for the massless Schwinger model.

To integrate the gauge links we first start by performing a character expansion on the Boltzmann factor corresponding to the pure gauge plaquette action,

$$e^{-\beta\cos\left[A_\mu(x)+A_\nu(x+\mu)-A_\mu(x+\nu)-A_\nu(x)\right]} = \sum_{m=-\infty}^{m=\infty} I_m(-\beta)e^{im\left[A_\mu(x)+A_\nu(x+\mu)-A_\mu(x+\nu)-A_\nu(x)\right]}. \quad (11)$$

Each plaquette p is now labeled by an integer m_p. Note that $I_m(-\beta) = (-1)^m I_m(\beta)$. Furthermore, each link l is shared by two plaquettes p and p' each of which supplies a factor of $e^{im_pA_l}$ and $e^{-im_{p'}A_l}$. In addition, the link carries a factor of $e^{ik_lA_l}$ or $e^{-i\bar{k}_lA_l}$ coming from Z_F. Thus, in total, links carry two m indices inherited from their neighboring plaquettes together with a k and a $\bar{k}$ index associated with the fermionic hopping terms. The integral over the link field then gives

$$\int_{-\pi}^{\pi}\frac{dA_l}{2\pi}e^{i(m_p-m_{p'}+k_l-\bar{k}_l)A_l} = \delta_{m_p-m_{p'}+k_l-\bar{k}_l,0}. \quad (12)$$

This allows us to write the partition function as

$$Z = \sum_{\{m_p\}}\sum_{\{k_l,\bar{k}_l\}}\prod_l \delta_{m_p-m_{p'}+k_l-\bar{k}_l,0}\prod_p I_{m_p}(\beta) \times \prod_x T^x_{k_1\bar{k}_1k_2\bar{k}_2k_3\bar{k}_3k_4\bar{k}_4}\times(-1)^{N_L+N_P+\frac{1}{2}\sum_\ell L(\ell)}, \quad (13)$$

where $\{m_p\}$ denotes the set of plaquette integers over the entire lattice, $\{k_l,\bar{k}_l\}$ represent k indices over the links, and $N_P = \sum_p m_p$. At this point we have included all the minus signs for completeness. For periodic boundary conditions, the sum of winding numbers must always be zero, since one is restricted to the total charge-0 sector of the theory. Note that for this situation the overall Z_2 factor (±1) in Eq. (8) is always positive [23].

Now, associated with each link are m fields and k fields, and a constraint between them. Associated with each plaquette is a single m field. This lets us define a link tensor, and a plaquette tensor. Link tensors have indices connecting to fermion tensors (the T tensors) living on each site, and guage-field indices connecting to plaquette tensors (on each plaquette). We define this link tensor, A, as,

$$A_{m_im_jk_a\bar{k}_ak_b\bar{k}_b} \equiv \delta_{m_i-m_j+k_a-\bar{k}_a,0}\delta_{k_a,k_b}\delta_{\bar{k}_a,\bar{k}_b}. \quad (14)$$

Here m_i and m_j are plaquette numbers associated with the surrounding plaquettes to the link, and the k indices are the k and $\bar{k}$ indices on that link from Eq. (12). The fermionlike indices on link tensors are purely diagonal as seen from the definition involving the δ function constraints on links. A diagram showing the relative position of the fermion and plaquette indices is shown in Fig. 2(b). Since there is only a single m associated with each plaquette, a tensor definition must only depend on that single m. A plaquette tensor, B, can be defined as,

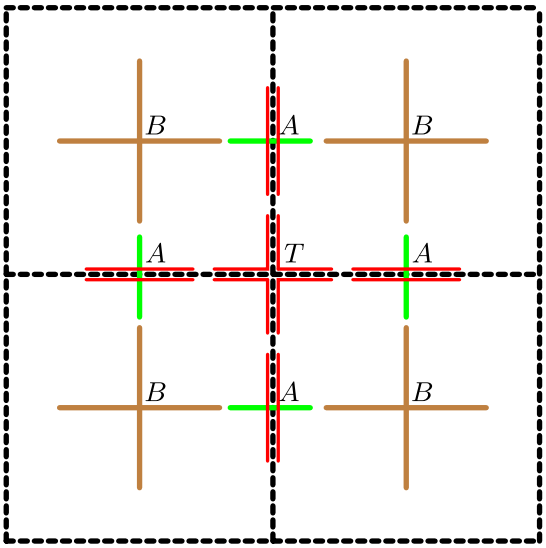

FIG. 3. Elementary tensors T, A, and B. When these tensors are contracted in the pattern shown here the world-line representation of the partition function is generated exactly.

$$B_{m_1m_2m_3m_4} = \begin{cases} I_m(\beta) & \text{if } m_1=m_2=m_3=m_4=m \\ 0 & \text{otherwise,}\end{cases}, \quad (15)$$

where the subscripts 1, 2, 3, and 4 simply denote the four surrounding link indices on the A tensors and are not explicitly associated with directions, since the tensor is completely diagonal. A graphical representation for the B tensor associated with plaquettes is shown in Fig. 2(c).

These definitions of the A and B tensors allow us to write the partition function as follows:

$$Z = \sum_{\{k,\bar{k}\}}\sum_{\{m_p\}}\left(\prod_p B_{m_im_jm_km_l}\right)\left(\prod_l A_{m_im_jk_a\bar{k}_ak_b\bar{k}_b}\right) \times\left(\prod_x T_{k_a\bar{k}_ak_b\bar{k}_bk_c\bar{k}_ck_d\bar{k}_d}\right). \quad (16)$$

This contraction over three unique tensor types can be represented as the tensor network shown in Fig. 3. Since the fermionic k indices always come in k, $\bar{k}$ pairs, we can form a product state of those two indices to reduce the complexity of the notation,

$$T \to T' = T_{(k_a \otimes \bar{k}_a)(k_b \otimes \bar{k}_b)(k_c \otimes \bar{k}_c)(k_d \otimes \bar{k}_d)} = T_{K_a K_b K_c K_d} \tag{17}$$

$$A \to A' = A_{m_i m_j (k_a \otimes \bar{k}_a)(k_b \otimes \bar{k}_b)} = A_{m_i m_j K_a K_b}. \tag{18}$$

The new enlarged K indices take values from 0 to 3, enumerating the four possible states each link can have unoccupied, incoming, outgoing, and dimer. The A tensors are still diagonal in the new K indices.

III. TRANSFER MATRIX

Using the tensors defined in the previous sections, one can build a transfer matrix for this model. The transfer matrix can be defined as the product of two types of matrices. In this section, we first define and construct these two different matrices. Then, by combining these two matrices in the appropriate way we can define a transfer matrix. The partition function is the trace of the N_τ^{th} power of this final matrix.

The first type of matrix we define is the $\mathcal{B}$ matrix. It is made by contracting alternating B and A tensors along a time slice,

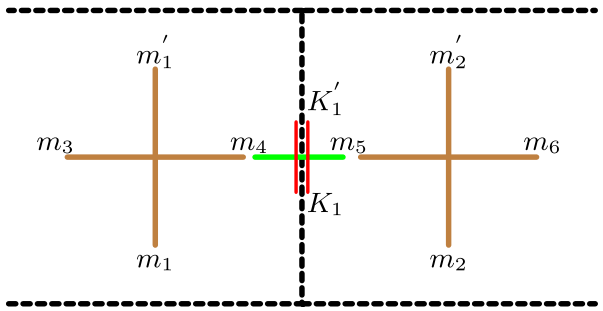

FIG. 4. Construction of part of the $\mathcal{B}$ matrix. In principle the construction continues to the left and right with A tensors contracted with the B tensors, and so on.

$$\mathcal{B}_{(m_1 \otimes \cdots m_N \otimes K_1 \otimes \cdots K_N)(m_1' \otimes \cdots m_N' \otimes K_1' \otimes \cdots K_N')} = B_{mm'm_1m_1'} A_{m'm''K_1K_1'} B_{m''m'''m_2m_2'} \times A_{m'''m''''K_2K_2'} \cdots B_{m^{(N-1)}mm_Nm_N'}, \tag{19}$$

where a sum over repeated indices is implied. Diagrammatically $\mathcal{B}$ is represented as Fig. 4. An important feature of this matrix is that it is diagonal, due to the diagonal nature of the B tensors, and the K indices in the A tensors. This means incoming states through this matrix do not change into other states.

In analogy with the construction of $\mathcal{B}$ we define the $\mathcal{A}$ matrix as the alternating contraction of T and A tensors along a time slice,

$$\mathcal{A}_{(m_1 \otimes \cdots m_N \otimes K_1 \otimes \cdots K_N)(m_1' \otimes \cdots m_N' \otimes K_1' \otimes \cdots K_N')} = A_{m_1 m_1' \bar{K}_1 \bar{K}_2} T_{\bar{K}_2 \bar{K}_3 K_1 K_1'} A_{m_2 m_2' \bar{K}_3 \bar{K}_4} \cdots A_{m_N m_N' \bar{K}_N \bar{K}_1} \tag{20}$$

with a diagrammatic representation given by Fig. 5. This matrix has off diagonal elements and is responsible for the changing of states between time slices. This matrix moves fermionic current across space, and through time, with the appropriate shift in the electric field to balance.

Using the definitions above we can recast the partition function into an alternating product of $\mathcal{B}$ and $\mathcal{A}$ matrices. This alternating product can be broken up and recast as the N_τ^{th} power of a single matrix,

$$\mathcal{T}_{\alpha\beta} = \sqrt{\mathcal{B}}_{\alpha\delta} \mathcal{A}_{\delta\gamma} \sqrt{\mathcal{B}}_{\gamma\beta}, \tag{21}$$

where the square root is well-defined since $\mathcal{B}$ is diagonal in all of its indices (and its matrix elements are positive). The indices in Eq. (21) are collective indices as defined before in the definitions of the $\mathcal{B}$ and $\mathcal{A}$ tensors. Now we can write the partition function as follows:

$$Z = \text{Tr}[\mathcal{T}^{N_t}]. \tag{22}$$

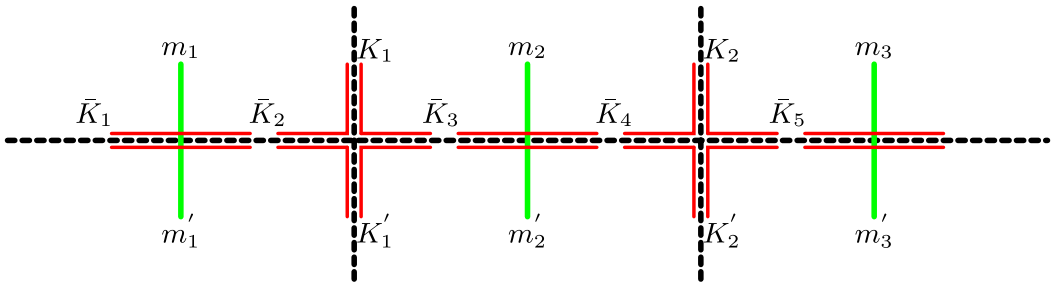

FIG. 5. Construction of matrix $\mathcal{A}$. In principle the construction continues to the left and right, alternating contraction between A and T tensors. This matrix is responsible for moving fermionic current around in space and time, and adjusting the gradient of the electric field to compensate.

IV. FUNDAMENTAL TENSOR FOR TRG

A. Asymmetric tensor

In order to have efficient numerical calculations using the TRG, the tensor network structure should be translationally invariant. This means that for whatever fundamental tensor one uses, it must contract naturally with itself. That is, the top indices of the fundamental tensor should be compatible for contraction with the bottom indices, and the indices on the left side of the tensor should be compatible for contraction with the indices on the right.

For this goal, we define a tensor, $\mathcal{M}$, using a single elementary plaquette tensor (the B), two link tensors (the As), and a single fermion T tensor. This is shown diagrammatically in Fig. 6. As can be seen from the figure, there are two different types of indices associated with each direction in the tensor. Each direction has one m index, and one K index. However, repeated contraction of this tensor with itself in the appropriate pattern reproduces the partition function. This is the only fundamental tensor necessary to do that. The tensor is then explicitly given as,

$$\mathcal{M}_{m_1m_2m_3m_4K_1K_2K_3K_4} = \sum_{m_1',m_2',\bar{K}_1,\bar{K}_2} B_{m_1m_1'm_2m_2'} \times A_{m_2'm_3K_1\bar{K}_1} T_{\bar{K}_1K_2\bar{K}_2K_3} A_{m_4m_1'\bar{K}_2K_4}. \tag{23}$$

Here the K indices always have dimension four, however the m indices run over all integers. The m indices are constrained by the K indices though. Looking at a single direction, the total size of the state-space associated with two of the indices is $N_{\text{gauge}} \times 4$, where N_{gauge} is the number of states allowed for the B tensor index in practice.

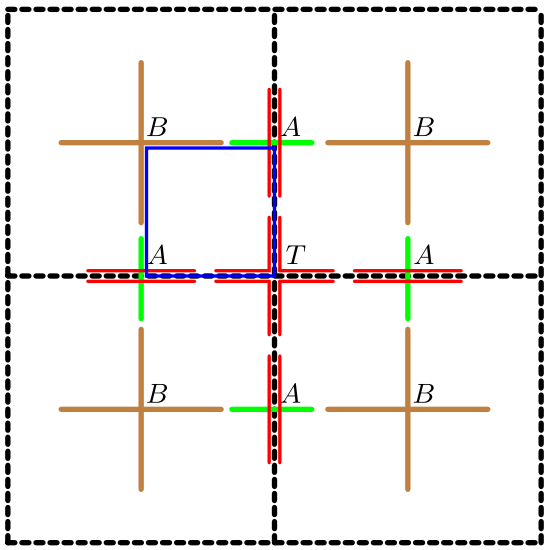

FIG. 6. Construction of tensor $\mathcal{M}$ shown as the four tensors sharing the blue loop. This is a possible single tensor which can be contracted with itself recursively to generate the partition function.

B. Symmetric tensor

It is possible to form a completely symmetric tensor in both space and time, as opposed to the asymmetric tensor constructed above. This tensor formulation relies on "dressing" the link fermion tensors in their surrounding gauge field configurations. This is possible because of how the B tensor is completely diagonal in its four indices.

To construct the symmetric tensor, the first step is to separate the B tensor into eight smaller pieces, four of which are associated with the adjacent link tensors, and the other four are associated with the four adjacent site tensors,

$$\begin{aligned} B_{m_1m_2m_3m_4} &= \sum_{\alpha,\beta,\gamma,\sigma} b_{m_1\sigma\alpha} b_{m_2\alpha\beta} b_{m_3\beta\gamma} b_{m_4\gamma\sigma} \\ &= \sum_{\alpha,\beta,\gamma,\sigma,\rho,\lambda,\chi,\psi} b_{m_1\psi\alpha}\delta_{\alpha\beta} b_{m_2\beta\gamma}\delta_{\gamma\sigma} b_{m_3\sigma\rho}\delta_{\rho\lambda} b_{m_4\lambda\chi}\delta_{\chi\psi}. \end{aligned} \tag{24}$$

The b tensors are also diagonal, and the δ matrices are simply Kronecker deltas. This decomposition can be seen graphically in Fig. 7. In principle, each of the above sums runs over all the integers; however, in practice one is forced to restrict the sum.

The b tensors are contracted with adjacent A tensors, and the Kronecker deltas are moved to the surrounding site tensors. The new A tensors, $\tilde{A}$, are given by

$$\tilde{A}_{(m_1Km_2)(m'_1K'm'_2)} = \sum_{\alpha,\beta} b_{\alpha m_1 m'_1} A_{\alpha\beta KK'} b_{\beta m_2 m'_2}. \tag{25}$$

This $\tilde{A}$ matrix is diagonal, since it is diagonal in all three sets of indices (the Ks, and the ms) due to the aforementioned diagonal nature of the B tensor and the already diagonal nature of the K indices in the A tensor. This tensor can be seen in Fig. 8.

For the site tensor (T tensor), we now "wrap" it in Kronecker deltas which enforce that all four site tensors around a plaquette have the same m-plaquette number associated with that plaquette. The new $\tilde{T}$ tensor has the form,

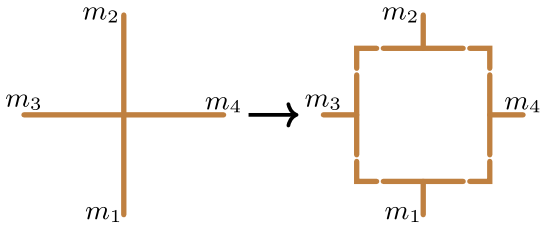

FIG. 7. A graphical representation of how the decomposition of the B tensor takes place. Each smaller tensor is also diagonal so that all m indices must take on the same values.

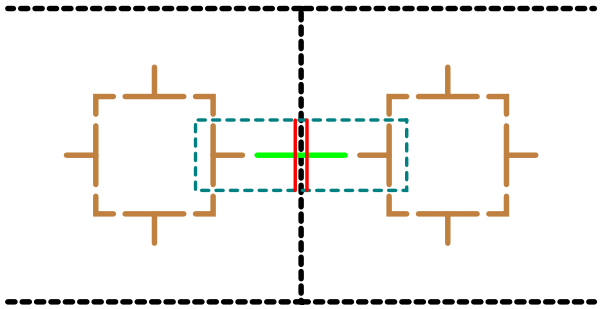

FIG. 8. The modified $\tilde{A}$ tensor (boxed in teal), built from the original A tensor, and the b tensors from the decomposition of the two B tensors on the adjacent plaquettes.

$$\tilde{T}_{(m_1K_1m_8)(m_4K_2m_5)(m_2K_3m_3)(m_6K_4m_7)} = T_{K_1K_2K_3K_4}\delta_{m_1m_2}\delta_{m_3m_4}\delta_{m_5m_6}\delta_{m_7m_8}, \tag{26}$$

and can be seen in Fig. 9. At this point, there are no B tensors remaining. The partition function is simply a contraction of the $\tilde{A}$ and $\tilde{T}$ tensors. To construct a single, symmetric, translation invariant tensor, we split the diagonal $\tilde{A}$ into two halves using the singular value decomposition,

$$\begin{aligned}\tilde{A}_{IJ} &= \sum_{\alpha,\beta} U_{I\alpha}\lambda_{\alpha\beta}U^{\dagger}_{\beta J} \\ &= \sum_{\alpha,\beta,\gamma}\left(U_{I\alpha}\sqrt{\lambda_{\alpha\beta}}\right)\left(\sqrt{\lambda_{\beta\gamma}}U^{\dagger}_{\gamma J}\right) \\ &= \sum_{\alpha} L_{I\alpha}L^{\dagger}{}_{\alpha J}.\end{aligned} \tag{27}$$

Furthermore, there are singular values with value zero, and they can be removed to decrease the size of the state space. This is equivalent to taking the square-root of the $\tilde{A}$ matrix and removing the zero columns (rows). With the L matrices we can now form a symmetric tensor, by contracting four of these matrices with a $\tilde{T}$,

$$S_{ijkl}(\beta) = \sum_{\alpha,\beta,\gamma,\delta}\tilde{T}_{\alpha\beta\gamma\delta}L_{\alpha i}L_{\beta j}L_{\gamma k}L_{\delta l}. \tag{28}$$

This tensor is symmetric in space and time, and since the L matrices are diagonal, its nonzero tensor elements are constrained by the fermion tensor, T. This final S tensor satisfies the same constraint as the original fermion T tensor, however with tensor elements with values other than 1, instead given by linear combinations of modified Bessel functions which are functions of the gauge coupling.

V. NUMERICAL SIMULATION: HOTRG AND HYBRID MONTE CARLO

We implemented the HOTRG algorithm to evaluate $\ln Z$ using the tensor defined in Eq. (23) as a translation invariant tensor for coarse-graining. At each step of the coarse-graining process, the HOTRG attempts to minimize the difference between the norms of the approximate tensor, and the tensor that would result from an exact contraction at that step. This is the only criteria which is used to determine the tensor at each step. This is in contrast to the original tensor renormalization group [1] which uses the singular value decomposition to approximate the bonds between blocks, and Refs. [11–15] which attempt to remove the local entanglement between blocks.

We measured the average plaquette,

$$\langle U_P\rangle = \frac{1}{V}\frac{\partial \ln Z}{\partial\beta}, \tag{29}$$

as a function of the gauge coupling and compared it to numerical data from Ref. [24]. In this case our computation using HOTRG completely agrees with the worm algorithm generated data. Moreover we can add a Θ term to the original action which results in new couplings, expressed as linear combinations of the gauge coupling and theta parameter, $\eta = \frac{\beta}{2} - \frac{\Theta}{4\pi}$ and $\bar{\eta} = \frac{\beta}{2} + \frac{\Theta}{4\pi}$. For the tensor construction here we only need to redefine the plaquette tensor, B, with $I_m(\beta)$ replaced by $I_m(2\sqrt{\eta\bar{\eta}})(\eta/\bar{\eta})^{m/2}$.

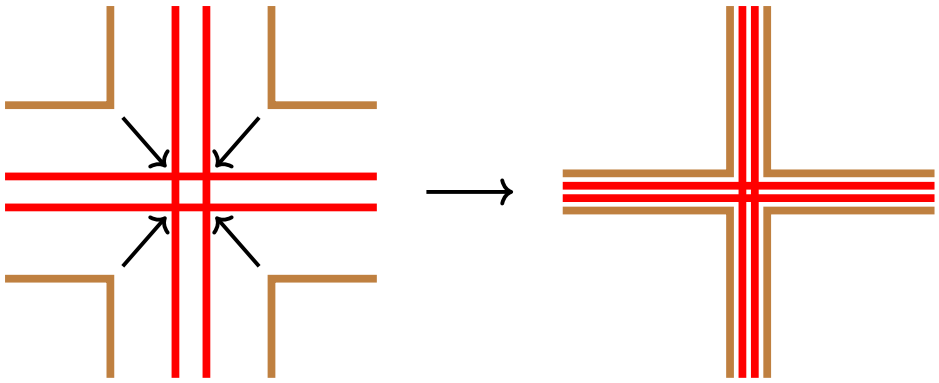

FIG. 9. The modified fermion tensor. The corners of the decomposed B tensor are moved to the T tensor at each site. These corners are Kronecker deltas, and enforce that each site around a plaquette has the same plaquette quantum m number.

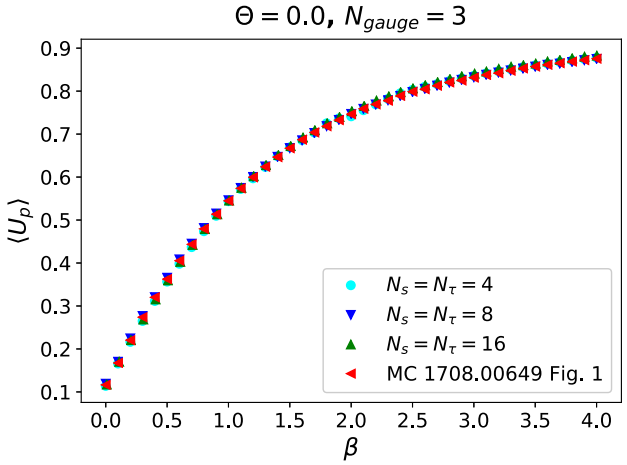

FIG. 10. Average Plaquette vs β for lattice sizes with $N_\tau = N_s = 4$, 8, and 16 and compared with Monte Carlo data from Ref. [24]. For this data $N_{\text{gauge}} = 3$ is sufficient to achieve similar accuracy to MC data. Here $D_{\text{bond}} = 40$ states.

To ensure the formulation is valid, we measured a couple of observables, including the average plaquette $\langle U_p \rangle$, and the topological charge density, $\langle Q \rangle$ as a function of the Θ parameter. The topological charge density is defined as

$$\langle Q \rangle = -\frac{1}{V}\frac{\partial \ln Z}{\partial \Theta}. \tag{30}$$

The results of the calculation of the average plaquette as a function of β for different system sizes can be seen in Fig. 10 and as a function of Θ in Fig. 11. If the final number of states kept associated with each tensor index is D_{bond}, we typically kept a $D_{\text{bond}} \simeq 40$ and looked for convergence in a window of 40–50 states. We find good agreement and convergence across a wide range of β values for the relatively small number of gauge states, $N_{\text{gauge}} = 3$ and 5.

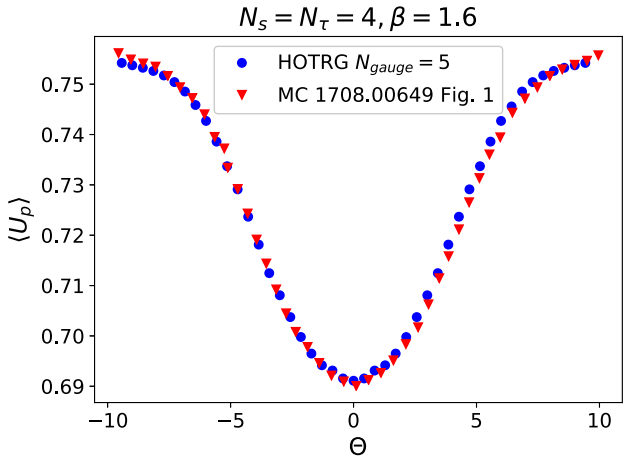

FIG. 11. Average Plaquette vs Θ for a lattice with $N_s = N_\tau = 4$. Here $N_{\text{gauge}} = 5$ is necessary to achieve similar accuracy to the MC data. Here a $D_{\text{bond}} = 40$ was used.

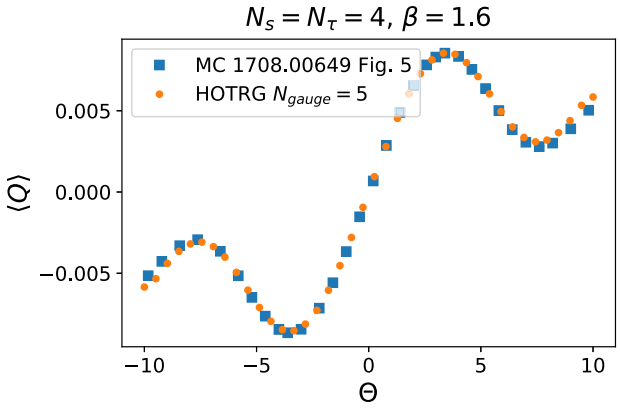

FIG. 12. The topological charge density as a function of Θ. Here we compare with Monte Carlo data from Ref. [24]. We find a slightly larger range of plaquette quantum numbers are necessary—in contrast to the average plaquette—to achieve consistent results. In this case, the plaquette numbers had to be allowed to run from $m = -2$ to 2. A $D_{\text{bond}} = 50$ was used in this case.

The results for the topological charge density can be seen in Fig. 12, and again we find good agreement across the range scanned, however to obtain this result a larger $N_{\text{gauge}} = 5$ was necessary.

However, we have also observed that for large Θ and β values, the results on larger volumes were *significantly* more noisy. It appeared one would need a final $D_{\text{bond}} > 60$ at least. There appear to be two possible reasons for this problem; a failure of the (truncated) character expansion to capture the effects of the topological term or specific problems associated with the staggered fermions in this model. To try to diagnose the problem further we have additionally studied the Abelian Higgs model in the presence of the same topological term.

VI. THE ABELIAN HIGGS MODEL WITH A TOPOLOGICAL TERM

Motivated by the poor signal-to-noise ratio in larger volume calculations of topological observables in the Schwinger model, we attempted to understand the source of the noise. On the one hand, perhaps the HOTRG is unable to capture the important states (as mentioned above) due to the fact that the truncation scheme is unaware of which fermion winding numbers are valid and important in the final partition function. On the other hand, perhaps the topological nature itself is difficult to capture with only a local tensor. In order to investigate whether the fermionic nature is the source of difficulty, or the topological nature, we studied the Abelian Higgs model with a topological term. This model is formally similar to the Schwinger model; with the fermionic fields essentially replaced by bosonic ones.

The work in this section is not meant to be exhaustive, and other works on this model have been carried out in the

past [6,44,45]. Instead, the goal was to identify if the HOTRG algorithm has difficulty with capturing topological information of field configurations during truncation, or if the fermion tensor formulation used here may be the cause of difficulty.

A. The model

We consider the Abelian Higgs model in $1+1$ Euclidean dimensions,

$$S = S_\beta + S_\lambda + S_\kappa + S_\Theta \tag{31}$$

with S_β the same as before, and

$$\begin{aligned} S_\lambda &= \sum_x (\lambda(|\phi_x|^2 - 1)^2 + |\phi_x|^2) \\ &= \sum_x (\lambda(\rho_x^2 - 1)^2 + \rho_x^2) \end{aligned} \tag{32}$$

is the Higgs potential with $\phi_x = \rho_x e^{i\theta_x}$ a complex scalar field, $\rho_x \geq 0$, and λ a real number. In addition, there is a matter-gauge interaction given by

$$\begin{aligned} S_\kappa &= -2\kappa \sum_{x,\mu} \Re[\phi_x^* U_{x,\mu} \phi_{x+\hat{\mu}}] \\ &= -2\kappa \sum_{x,\mu} \rho_x \rho_{x+\hat{\mu}} \cos(\theta_{x+\hat{\mu}} - \theta_x + A_{x,\mu}) \end{aligned} \tag{33}$$

with $U_{x,\mu} = e^{iA_{x,\mu}}$ the lattice link parallel transport with $A_{x,\mu}$ the vector potential and κ a real number. Finally, we include a topological term,

$$S_\Theta = i\frac{\Theta}{2\pi} \sum_x \mathrm{Im}[U_P] \tag{34}$$

with Θ a real number, and U_P given as before from Sec. II.

We consider this action in the limit $\lambda \to \infty$. In this limit, the length of the Higgs field is forced to one, and the Higgs potential can be ignored as an overall shift in the action. This leaves only the Goldstone modes of the Higgs field. Since U_P is a gauge-invariant combination of link variables, we can perform a change of variables such that $A'_{x,\mu} \equiv A_{x,\mu} + \theta_{x+\hat{\mu}} - \theta_x$. This leaves S_β and S_Θ unchanged, however simplifies the matter-gauge term,

$$S_\kappa \to S'_\kappa = -2\kappa \sum_{x,\mu} \cos(A_{x,\mu}{}'), \tag{35}$$

where we will drop the prime in what follows for convenience.

B. Dual variables and tensor definitions

Dual variable formulations for this model have been given with, and without, a topological term in a variety of ways [45,46]. Here we give a review of the derivation in the presence of a topological term.

The partition function for this model is given by (ignoring the overall constant out front from the Higgs field integration),

$$Z = \int D[A] e^{-S_\beta - S_\Theta - S_\kappa}. \tag{36}$$

The two terms with U_p can be Fourier expanded,

$$\prod_x e^{\beta \cos F_{x,12} - i\frac{\Theta}{2\pi} \sin F_{x,12}} = \prod_x \sum_{m_{x,12}=-\infty}^{\infty} C_{m_{x,12}}(\beta, \Theta) e^{i m_{x,12} F_{x,12}}. \tag{37}$$

Similarly with the matter-gauge term,

$$\prod_{x,\mu} e^{2\kappa \cos(A_{x,\mu})} = \sum_{n_{x,\mu}=-\infty}^{\infty} I_{n_{x,\mu}}(2\kappa) e^{i n_{x,\mu} A_{x,\mu}}. \tag{38}$$

Here the Cs can be solved for numerically, or analytically [45], and the Is are the modified Bessel functions.

By expanding this way, we are able to carry out the A integrations exactly at each link. These integrations give a new, constrained, partition function,

$$Z = \sum_{\{m\}} \sum_{\{n\}} \left(\prod_x C_{m_{x,12}}(\beta, \Theta) \right) \left(\prod_{x,\mu} I_{n_{x,\mu}}(2\kappa) \delta_{n_{x,\mu}, \epsilon_{\mu\nu} \Delta_\nu m_{x,12}} \right). \tag{39}$$

In this partition function, the n fields on the links are constrained to equal the difference in the bounding-plaquette m fields on the sides. In fact, the n summations can be carried out because of the constraint, and the partition function can be simply written as

$$Z = \sum_{\{m\}} \left(\prod_x C_{m_{x,12}}(\beta, \Theta) \right) \left(\prod_{x,\mu} I_{\epsilon_{\mu\nu} \Delta_\nu m_{x,12}}(2\kappa) \right). \tag{40}$$

With this formulation, we can again define tensors on the links, and on the plaquettes (none on the sites) of the lattice in a similar way to before with the Schwinger model.

We define the B tensor as

$$B_{m_1 m_2 m_3 m_4} \equiv \begin{cases} C_m(\beta, \Theta) & \text{if } m = m_1 = m_2 = m_3 = m_4 \\ 0 & \text{otherwise,} \end{cases} \tag{41}$$

and the A tensor as

$$A_{mm'} \equiv I_{|m-m'|}(2\kappa). \tag{42}$$

The A and B tensors here are similar to those from the Schwinger model described above. For the B tensor, only the weight associated with the plaquette is different; however it is still totally diagonal. For the A tensor, the

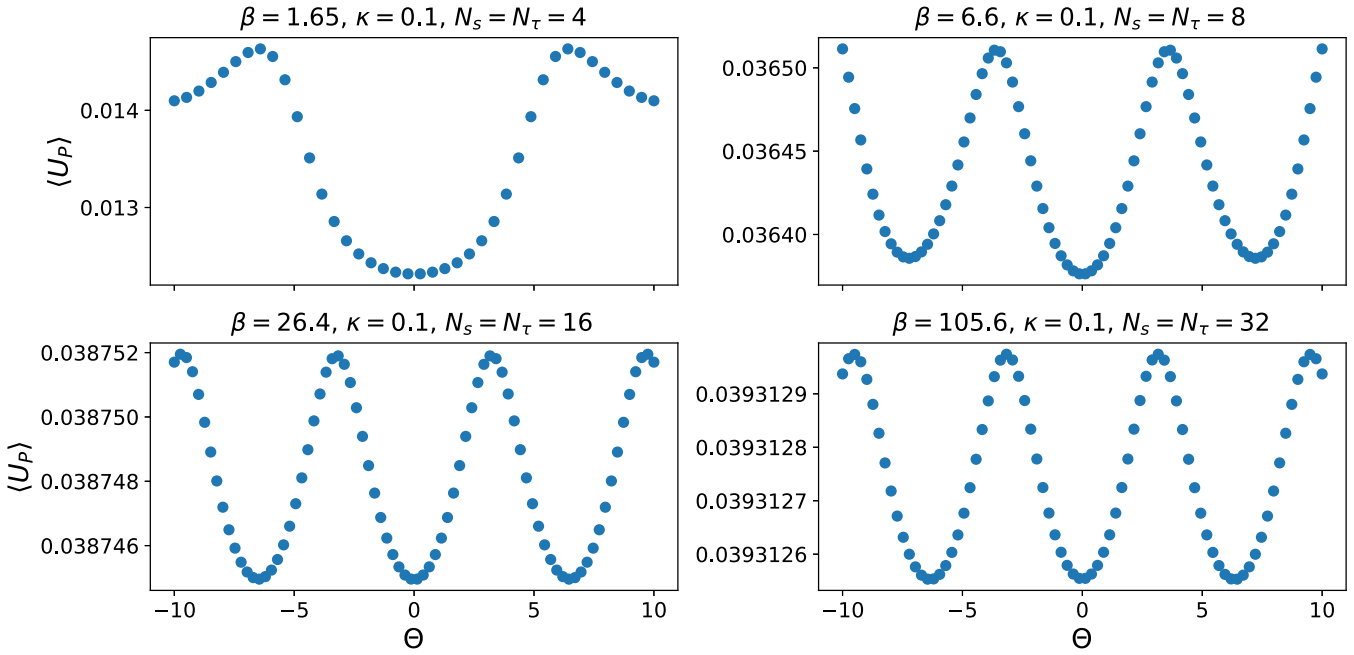

FIG. 13. The continuum limit of the average plaquette, Eq. (29), as a function of the Θ parameter. The expected 2π periodicity is tending to restoration for larger volumes. Here a $D_{\text{bond}} = 40$ was used.

fermionic indices are missing from the definition, and the A tensor is simply a matrix in this case, with elements given by the modified Bessel functions. The partition function is then written with a tensor trace as

$$Z = \mathrm{Tr}\left[\prod_x B^{(x)} \prod_{x,\mu} A^{(x,\mu)}\right], \tag{43}$$

which implies contracting all the tensor indices appropriately.

Constructing a fundamental tensor can be carried out in an identical fashion to that in Ref. [6]. The A matrix can be square-rooted, $A = LL^T$, and four L matrices can be contracted with a single B tensor to form the basic fundamental tensor,

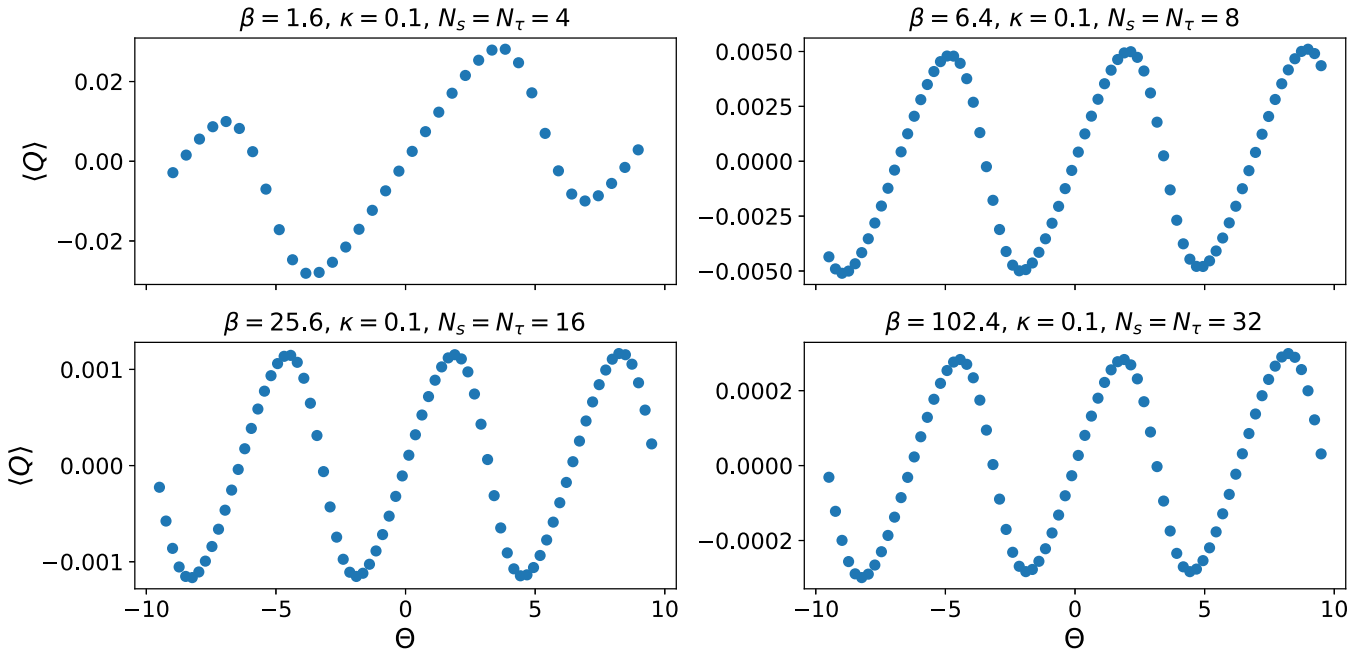

FIG. 14. The continuum limit of the topological charge density. This reveals that $\langle S_\Theta/\Theta \rangle$ tends to a constant in the continuum limit. We also see the restored 2π periodicity for larger volumes. Here a $D_{\text{bond}} = 40$ was used.

$$T_{ijkl} = \sum_{\alpha,\beta,\gamma,\delta} B_{\alpha\beta\gamma\delta} L_{\alpha i} L_{\beta j} L_{\gamma k} L_{\delta l}. \tag{44}$$

Contraction of this tensor with itself repeatedly, in the geometry of the lattice, reproduces the partition function given in Eq. (43).

C. Tensor calculations

Using the tensor formulation from above, we can calculated the quantity $\ln Z$ using the HOTRG. From that, bulk thermodynamic quantities can be derived. We considered the same quantities from the Schwinger model defined in Eqs. (29) and (30). Again, we kept a number of states, D_{bond}, in a window of 40–50 for the calculations mentioned below. This was sufficient for convergence.

In Fig. 13 we see the continuum limit of the average plaquette [Eq. (29)] keeping β/V fixed. In the continuum, infinite-volume limit the partition function is periodic in Θ, and hence one expects to see expectation values show this same periodicity. One can see the periodicity restored as the continuum limit is taken in Fig. 13.

In Fig. 14 the topological charge density, $\langle Q \rangle$, as a function of Θ is plotted while taking the continuum limit. Here we see the amplitude decrease by approximately a factor of 4 for each increase by a factor of 4 in the volume. This indicates that $\langle Q \rangle V$ approaches a constant while taking the continuum limit. Also, similarly to $\langle U_P \rangle$, one can see the 2π periodicity restored in the continuum limit.

From these two observables, already it is clear that the Abelian Higgs model in the presence of a topological term is accessible using the tensor renormalization group and the HOTRG algorithm. The data appear smooth and converge, in contrast to the Schwinger model on a 8×8 lattice. This lends evidence to the option that the noisy data in the Schwinger model while taking the continuum limit arise in some way from the fermion fields and not the topological term.

VII. CONCLUSIONS

In this paper we have constructed a tensor network formulation of the massless lattice Schwinger model with staggered fermions. We have considered both the usual action and one in which a topological term is added. The addition of the latter term induces a sign problem and renders the model intractable for a conventional hybrid Monte Carlo simulation.

We used a bosonic version of the HOTRG algorithm (the original version), as opposed to a Grassmann version of the algorithm [18–20]. This is only possible because the fermions are completely integrated out of the model from the very beginning, the partition function is left without a sign-problem and can be computed entirely from local information.

Using the HOTRG algorithm we have computed the free energy and its derivatives and compared the results, where possible, with both hybrid Monte Carlo simulations and simulations based on a dual representation based on fermion loops. Where comparison is possible the agreement is good with the tensor network calculation being superior computationally to Monte Carlo simulations. That said, we have experienced difficulties measuring observables for large values of the topological coupling, Θ, and large values of the gauge coupling, β, as the volume is increased. Typically the signal for an operator like the plaquette becomes very noisy after several iterations of the blocking scheme.

A possible explanation is that the arguments used for the positivity of terms in the sum of the partition function assume a complete lattice with boundary conditions and lattice size already achieved [23]. In contrast, the HOTRG does not know beforehand what the final size of the lattice will be, or what the boundary conditions will be at that size. This in turn gives the algorithm more freedom to choose which states are relevant during truncation, even though those very states may be projected out in the final step of blocking, rendering them useless.

A tensor construction scheme which uses an environment tensor might achieve better results at larger volumes, since, the forward-backward iteration from a complete lattice should retroactively adjust the intermediate states kept during truncation at smaller volumes. Alternatively, the Grassmann (HO)TRG could be used. It incorporates the fermion field integration at each truncation step, as opposed to the method used here where the fermion fields are integrated out exactly.

Of course in the continuum limit the Dirac operator of the massless Schwinger model develops chiral zero modes in the background of gauge fields with nontrivial topology ensuring that such configurations do not contribute to the path integral and thereby removing the Θ dependence of the free energy. It is logically possible that the problems encountered in the renormalization group calculation of the model has its origins in this fact—the noisy dependence on Θ being the best the truncated system can do to replicate an independence of the free energy on Θ.

The Θ dependence is restored in the presence of a fermion mass. However in that case there are nontrivial -1 factors which appear in the dual representation of the partition function. Part of the phase depends on the number of closed fermion loops appearing in any particular dual configuration. It is extremely hard to see how this phase can be reconstructed from the contraction of local tensors in the formulation used here, and we have not been able to generalize the tensor network described here to the case of nonzero masses.

This should sound a cautionary note to the idea that tensor network formulations of lattice field theories are free of sign problems. In the case of fermion theories this may not be generically the case, and one may have to resort to other formulations, e.g., Grassmann (HO)TRG.

ACKNOWLEDGMENTS

The authors would like to thank the members of the QuLat Collaboration for stimulating discussions. S. C., Y. M., R. S., and J. U. Y. were supported by the U.S. Department of Energy (DOE) under Awards No. DE-SC0019139 and No. DE-SC0009998.

[1] M. Levin and C. P. Nave, Tensor Renormalization Group Approach to Two-Dimensional Classical Lattice Models, Phys. Rev. Lett. **99**, 120601 (2007).
[2] Y. Liu, Y. Meurice, M. P. Qin, J. Unmuth-Yockey, T. Xiang, Z. Y. Xie, J. F. Yu, and H. Zou, Exact blocking formulas for spin and gauge models, Phys. Rev. D **88**, 056005 (2013).
[3] D. Kadoh, Y. Kuramashi, Y. Nakamura, R. Sakai, S. Takeda, and Y. Yoshimura, Tensor network analysis of critical coupling in two dimensional ϕ^4 theory, J. High Energy Phys. 05 (2019) 184.
[4] A. Bazavov, S. Catterall, R. G. Jha, and J. Unmuth-Yockey, Tensor renormalization group study of the non-abelian higgs model in two dimensions, Phys. Rev. D **99**, 114507 (2019).
[5] J. F. Unmuth-Yockey, Gauge-invariant rotor hamiltonian from dual variables of 3d $u(1)$ gauge theory, Phys. Rev. D **99**, 074502 (2019).
[6] J. Unmuth-Yockey, J. Zhang, A. Bazavov, Y. Meurice, and S.-W. Tsai, Universal features of the Abelian Polyakov loop in $1+1$ dimensions, Phys. Rev. D **98**, 094511 (2018).
[7] J. Chen, H.-J. Liao, H.-D. Xie, X.-J. Han, R.-Z. Huang, S. Cheng, Z.-C. Wei, Z.-Y. Xie, and T. Xiang, Phase transition of the q-state clock model: Duality and tensor renormalization, Chin. Phys. Lett. **34**, 050503 (2017).
[8] S. Akiyama, Y. Kuramashi, T. Yamashita, and Y. Yoshimura, Phase transition of four-dimensional Ising model with higher-order tensor renormalization group, Phys. Rev. D **100**, 054510 (2019).
[9] S. Wang, Z.-Y. Xie, J. Chen, B. Normand, and T. Xiang, Phase transitions of ferromagnetic potts models on the simple cubic lattice, Chin. Phys. Lett. **31**, 070503 (2014).
[10] J. F. Yu, Z. Y. Xie, Y. Meurice, Y. Liu, A. Denbleyker, H. Zou, M. P. Qin, J. Chen, and T. Xiang, Tensor renormalization group study of classical xy model on the square lattice, Phys. Rev. E **89**, 013308 (2014).
[11] Z.-C. Gu and X.-G. Wen, Tensor-entanglement-filtering renormalization approach and symmetry-protected topological order, Phys. Rev. B **80**, 155131 (2009).
[12] M. Hauru, C. Delcamp, and S. Mizera, Renormalization of tensor networks using graph-independent local truncations, Phys. Rev. B **97**, 045111 (2018).
[13] S. Yang, Z.-C. Gu, and X.-G. Wen, Loop Optimization for Tensor Network Renormalization, Phys. Rev. Lett. **118**, 110504 (2017).
[14] A. Denbleyker, Y. Liu, Y. Meurice, M. P. Qin, T. Xiang, Z. Y. Xie, J. F. Yu, and H. Zou, Controlling sign problems in spin models using tensor renormalization, Phys. Rev. D **89**, 016008 (2014).
[15] G. Evenbly and G. Vidal, Tensor Network Renormalization, Phys. Rev. Lett. **115**, 180405 (2015).
[16] Z. Y. Xie, J. Chen, M. P. Qin, J. W. Zhu, L. P. Yang, and T. Xiang, Coarse-graining renormalization by higher-order singular value decomposition, Phys. Rev. B **86**, 045139 (2012).
[17] R. Sakai, S. Takeda, and Y. Yoshimura, Higher-order tensor renormalization group for relativistic fermion systems, Prog. Theor. Exp. Phys. (**2017**), 06.
[18] Y. Shimizu and Y. Kuramashi, Grassmann tensor renormalization group approach to one-flavor lattice Schwinger model, Phys. Rev. D **90**, 014508 (2014).
[19] Y. Shimizu and Y. Kuramashi, Critical behavior of the lattice Schwinger model with a topological term at $\theta = \pi$ using the Grassmann tensor renormalization group, Phys. Rev. D **90**, 074503 (2014).
[20] Y. Shimizu and Y. Kuramashi, Berezinskii-Kosterlitz-Thouless transition in lattice Schwinger model with one flavor of Wilson fermion, Phys. Rev. D **97**, 034502 (2018).
[21] S.Takeda and Y. Yoshimura, Grassmann tensor renormalization group for the one-flavor lattice GrossNeveu model with finite chemical potential, Prog. Theor. Exp. Phys. (**2015**), 04.
[22] D. Kadoh, Y. Kuramashi, Y. Nakamura, R. Sakai, S. Takeda, and Y. Yoshimura, Tensor network formulation for two-dimensional lattice $\mathcal{N}=1$ Wess-Zumino model, J. High Energy Phys. 03 (2018) 141.
[23] C. Gattringer, T. Kloiber, and V. Sazonov, Solving the sign problems of the massless lattice Schwinger model with a dual formulation, Nucl. Phys. **B897**, 732 (2015).
[24] D. Göschl, C. Gattringer, A. Lehmann, and C. Weis, Simulation strategies for the massless lattice Schwinger model in the dual formulation, Nucl. Phys. **B924**, 63 (2017).
[25] T. M. R. Byrnes, P. Sriganesh, R. J. Bursill, and C. J. Hamer, Density matrix renormalization group approach to the massive Schwinger model, Phys. Rev. D **66**, 013002 (2002).
[26] M. C. Bañuls, K. Cichy, J. I. Cirac, and K. Jansen, The mass spectrum of the Schwinger model with matrix product states, J. High Energy Phys. 11 (2013) 158.
[27] B. Buyens, F. Verstraete, and K. Van Acoleyen, Hamiltonian simulation of the Schwinger model at finite temperature, Phys. Rev. D **94**, 085018 (2016).
[28] B. Buyens, S. Montangero, J. Haegeman, F. Verstraete, and K. Van Acoleyen, Finite-representation approximation of lattice gauge theories at the continuum limit with tensor networks, Phys. Rev. D **95**, 094509 (2017).

[29] J. C. Pinto Barros, M. Dalmonte, and A. Trombettoni, String tension and robustness of confinement properties in the Schwinger-Thirring model, Phys. Rev. D **100**, 036009 (2019).
[30] L. Funcke, K. Jansen, and S. Kühn, Topological vacuum structure of the Schwinger model with matrix product states, Phys. Rev. D **101**, 054507 (2020).
[31] E. Ercolessi, P. Facchi, G. Magnifico, S. Pascazio, and F. V. Pepe, Phase transitions in Z_n gauge models: Towards quantum simulations of the Schwinger-Weyl QED, Phys. Rev. D **98**, 074503 (2018).
[32] G. Magnifico, M. Dalmonte, P. Facchi, S. Pascazio, F. V. Pepe, and E. Ercolessi, Real time dynamics and confinement in the $\mathbb{Z}_n$ Schwinger-Weyl lattice model for $1+1$ QED, arXiv:1909.04821.
[33] S. Kühn, J. Ignacio Cirac, and M.-C. Bañuls, Quantum simulation of the Schwinger model: A study of feasibility, Phys. Rev. A **90**, 042305 (2014).
[34] D. Yang, G. S. Giri, M. Johanning, C. Wunderlich, P. Zoller, and P. Hauke, Analog quantum simulation of $(1+1)$-dimensional lattice QED with trapped ions, Phys. Rev. A **94**, 052321 (2016).
[35] N. Klco, E. F. Dumitrescu, A. J. McCaskey, T. D. Morris, R. C. Pooser, M. Sanz, E. Solano, P. Lougovski, and M. J. Savage, Quantum-classical computation of Schwinger model dynamics using quantum computers, Phys. Rev. A **98**, 032331 (2018).
[36] E. Rico, T. Pichler, M. Dalmonte, P. Zoller, and S. Montangero, Tensor Networks for Lattice Gauge Theories and Atomic Quantum Simulation, Phys. Rev. Lett. **112**, 201601 (2014).
[37] C. Muschik, M. Heyl, E. Martinez, T. Monz, P. Schindler, B. Vogell, M. Dalmonte, P. Hauke, R. Blatt, and P. Zoller, U(1) Wilson lattice gauge theories in digital quantum simulators, New J. Phys. **19**, 103020 (2017).
[38] D. E. Kharzeev and Y. Kikuchi, Real-time chiral dynamics from a digital quantum simulation, arXiv:2001.00698.
[39] B. Chakraborty, M. Honda, T. Izubuchi, Y. Kikuchi, and A. Tomiya, Digital quantum simulation of the Schwinger model with topological term via adiabatic state preparation, arXiv:2001.00485.
[40] V. Kasper, F. Hebenstreit, F. Jendrzejewski, M. K. Oberthaler, and J. Berges, Implementing quantum electrodynamics with ultracold atomic systems, New J. Phys. **19**, 023030 (2017).
[41] F. M. Surace, P. P. Mazza, G. Giudici, A. Lerose, A. Gambassi, and M. Dalmonte, Lattice gauge theories and string dynamics in Rydberg atom quantum simulators, arXiv:1902.09551.
[42] C. J. Hamer, Z. Weihong, and J. Oitmaa, Series expansions for the massive Schwinger model in Hamiltonian lattice theory, Phys. Rev. D **56**, 55 (1997).
[43] By contrast, with the staggered discretization the Grassmann variables can be completely removed at the initial stage. This point is closely discussed later.
[44] D. R. T. Jones, J. Kogut, and D. K. Sinclair, Electrodynamics of the planar model: Its phase diagram, continuum limit, and mass spectrum, Phys. Rev. D **19**, 1882 (1979).
[45] C. Gattringer, T. Kloiber, and M. Müller-Preussker, Dual simulation of the two-dimensional lattice U(1) gauge-Higgs model with a topological term, Phys. Rev. D **92**, 114508 (2015).
[46] A. Bazavov, Y. Meurice, S.-W. Tsai, J. Unmuth-Yockey, and J. Zhang, Gauge-invariant implementation of the Abelian-Higgs model on optical lattices, Phys. Rev. D **92**, 076003 (2015).